Turkish Journal of Electrical Engineering & Computer Sciences

http://journals.tubitak.gov.tr/elektrik/

Research Article

Turk J Elec Eng & Comp Sci
(2019) 27: 1589 – 1602

doi:10.3906/elk-1809-98

Efficient features for smartphone-based iris recognition

Ritesh VYAS[1*], **Tirupathiraju KANUMURI**[2], **Gyanendra SHEORAN**[3], **Pawan DUBEY**[1]
[1]Department of Electronics and Communication Engineering, National Institute of Technology Delhi, Delhi, India
[2]Department of Electrical and Electronics Engineering, National Institute of Technology Delhi, Delhi, India
[3]Department of Applied Sciences (Physics), National Institute of Technology Delhi, Delhi, India

Received: 15.09.2018 • **Accepted/Published Online:** 18.02.2019 • **Final Version:** 15.05.2019

Abstract: Iris recognition has widely been used in personal authentication problems. Recent advances in iris recognition through visible wavelength images have paved the way for the use of this technology in smartphones. Smartphone-based iris recognition can be of significant use in financial transactions and secure storage of sensitive information. This paper presents a hybrid representation scheme for iris recognition in mobile devices. The scheme is called hybrid because it firstly makes use of Gabor wavelets to reveal the texture present in the normalized iris images, and then extracts statistical features from different partitions of Gabor-processed images. The standard mobile-iris database, called MICHE, is used for investigating the performance of the proposed approach. The comparison of the proposed approach with other widespread iris recognition approaches proves its efficacy.

Key words: Iris recognition, mobile devices, hybrid features, Gabor wavelets

1. Introduction

Iris has been the most popular biometric trait because of its uniqueness, permanence, and noninvasiveness [1]. It has found wide applications in border control [2], national ID schemes (e.g., Unique Identification Authority of India, available at https://uidai.gov.in/) and surveillance-based security services [3]. Additionally, performance of iris recognition systems is on par with that of another similar contenders like fingerprint, palmprint, and face [4].

Iris is the annular region of human eye which is delimited by two boundaries from either side: iris-pupil boundary and iris-sclera boundary. These boundaries are also called inner and outer boundaries, respectively, of the iris. Every human iris is characterized by a unique and discriminative texture that can be used to recognize people [5]. Moreover, iris of identical twins, and left and right irises of the same person, are also unique [6, 7].

The idea of iris recognition was first suggested by Flom and Safir [8]. They provided the conceptual design of an automated iris recognition system, which consisted of a highly constrained image acquisition framework. Later, first practical implementation of iris recognition was given by Daugman [1], who used the phase information of iris' texture to generate IrisCode. Daugman's IrisCode has been successfully used in many commercial iris recognition systems.

Since then, many researchers have tried in their own ways, to represent human iris in more distinctive manner. Masek [9] used the phase information of 1D log-Gabor filters to encode the iris patterns. Ganeshan et al. [10] used Laplacian of Gaussian (LOG) filter masks to construct Laplacian pyramids representation of the

*Correspondence: ritesh.vyas@nitdelhi.ac.in

iris image. Monro et al. [11] used DCT coefficients of half-overlapped patches of normalized iris images to form the feature vector. Miyazawa et al. [12] employed phase components of 2D discrete Fourier transform (DFT) of iris images to match iris images through band-limited phase only correlation (BLPOC).

Many contemporary approaches which aim at representing iris in several different ways have been reported. Rai and Yadav [13] proposed iris recognition through two-level Haar decomposition and 1D log-Gabor wavelet using SVM and Hamming distance as the classifiers. Tan and Kumar [14] utilized geometric key-based encoding of iris images. In another work by the same authors [15], iris was encoded with the help of phase information of Zernike moments and an exclusive phase-distance function was used for the matching purpose.

Bhateja et al. [16] used sparse representation to match iris images in k-nearest subspace. Umer et al. [17] proposed multiscale morphological features to extract features from iris images. Vyas et al. [18] used 2D Gabor filters with varying orientations to form a feature plane by performing Exclusive OR and summation operation on the Gabor-filtered images. Bansal et al. [19] represented the texture of iris using local principal independent components.

Subban et al. [20] employed Haralick features and optimized feature selection to efficiently represent the iris. Bansal et al. [21] utilized statistical features along radial and angular directions to get improved iris recognition. Poornima and Subramanian [22] employed log-Gabor filters for extracting iris features. Hamouchene and Aouat [23] proposed a neighborhood-based binary pattern to represent iris' texture efficiently. Vyas et al. [24] used GLCM features with varying offset distance value and classified them using artificial neural networks.

The mobile iris biometrics has found its way with MICHE I contest [25]. This contest was held for encouraging users to test iris segmentation techniques for images acquired from mobile devices. Iris segmentation is the process of localizing the boundaries of iris so that iris can be separated from rest of the eye image. After the successful completion of this contest, MICHE II contest was also organized, which targeted at the assessment of iris recognition techniques for mobile devices [26]. Many researchers from all over the globe participated in MICHE II and described various iris representation techniques [27–29].

The present work reports a hybrid feature extraction technique for mobile iris biometrics. The technique first exploits 2D Gabor wavelets at varying scales and orientations, to reveal the texture of iris images. Consequently, each Gabor-processed image is partitioned into subblocks to take the local features of iris into account. The subblocks at the first level of partitioning are kept to have same resolution. While, for second level of partitioning, the dimension of subblocks are chosen to have increased horizontal and vertical resolutions. This increased resolution of subblocks aid in countering the effects of eyelid and eyelash occlusions, present in the normalized iris image. After partitioning, the standard deviation is calculated for every subblock and feature vector is formed by storing the remainder after subtraction of standard deviations of lower- and higher-level subblocks. These feature vectors are further matched to find the degree of similarity between query and gallery images.

Rest of the paper is organized as follows. Section 2 explains the iris segmentation process employed in this paper while Section 3 provides a comprehensive explanation of the proposed feature extraction approach. Performance evaluation of the proposed approach is explicated in Section 4. Finally, the paper is concluded in Section 5.

2. Iris segmentation

As the mobile iris images are captured under uncontrolled frameworks, the image also contains other regions surrounding the iris region. For instance, the image may contain skin, cheek, portion of forehead, and hair. Therefore, it becomes necessary to first detect the eye region. In the present work, the eye region is detected using the Viola–Jones framework [30, 31]. This framework is based on extraction of rectangular features from the integral images of input eye image. As the iris images in MICHE database [25] are captured by the subject himself/herself, there are huge variations in the sizes of detected rectangular regions containing the iris. Therefore, the detected eye region is resized to a fixed dimension before proceeding further. Detection of eye region is depicted in Figure 1, where Figure 1a shows the original eye image and Figure 1b shows the detected eye (within red-colored box).

Figure 1. ROI extraction process: (a) Original image, (b) Detection of eye region using the Viola–Jones framework; marked within red box, (c) Iris segmentation with iris boundaries marked as green, (d) Corresponding iris mask, (e) Normalized iris, (f) Enhanced iris. (image source: 001_IP5_OU_F_RI_01_4.jpg).

Subsequently, the iris boundaries are localized following the method given by Zhao and Kumar [32]. Firstly, the eye images are processed through single-scale retinex technique to improve the color consistency. The color consistency can be defined as "the maintenance of color appearance despite variation in the color of nearby objects and despite variation in the spectral power distribution of the ambient light [33]". Therefore, color consistency plays a significant role while dealing with colored objects. In case of eye images, color consistency can directly affect the contrast between the iris/pupil and iris/sclera boundaries. Thereafter, relative total variation is defined for the whole image, which is minimized further using an L^1 norm minimization problem to divulge the structure of iris. The inner and outer boundaries of iris are then detected using circular Hough transform (CHT) approach [34] (refer to Figure 1c). The corresponding iris mask is then shown in Figure 1d. Lastly, the segmented iris region is transformed from rectangular to polar coordinates using Daugman's rubber sheet model [35] and the normalized iris is enhanced using common postprocessing steps [18]. The normalized and enhanced irises are shown in Figures 1e and 1f, respectively.

3. Proposed approach

As introduced in Section 1, the proposed scheme utilizes hybrid features of iris templates, which are constructed by using Gabor wavelet bank and simple statistical formulae. The features are referred to as hybrid due to the use of textural (Gabor) and statistical representations. The localized nature of iris features is taken into account by performing partitioning at two different levels. By doing so, effect of any global noise present in the iris image can be fended off. Additionally, the increased vertical and horizontal resolutions of second-level subblocks lead to cancellation of texture variations caused by eyelid and eyelash occlusions.

Algorithm 1 Hybrid features

Require: I : Normalized iris image

Ensure: FV : Feature vector containing hybrid features

1: Select red channel from I into I_1.

2: Design 2D Gabor wavelet bank using following equations:

$\Gamma(\alpha, n) = G(x, y, \sigma_\alpha, f_\alpha, \theta_n)$

$G(x, y, \sigma_\alpha, f_\alpha, \theta_n) = \frac{1}{\sqrt{2\pi\sigma_\alpha^2}} \exp\left\{-\frac{x^2+y^2}{\sigma_\alpha^2}\right\} \times \exp\left(2\pi i f_\alpha \left(x\cos\theta_n + y\sin\theta_n\right)\right)$ ▷ θ represents the orientation of Gabor filter; $1 \le \theta \le N$.

$f_\alpha = \frac{0.2592}{\sqrt{2^\alpha}}, \theta_n = \frac{n\pi}{4}, \quad \alpha = 0, 1, \ldots, 4, \quad n = 0, \ldots 3$

3: **for** $\alpha = 0$ to 4 **do**

4: **for** $n = 0$ to 3 **do**

5: Process I_1 with 2D Gabor wavelet through convolution operation: $F_{\alpha,n} = I_1 * \Gamma(\alpha, n)$

6: Partition the filtered image $F_{\alpha,n}$ at two levels ▷ Let $S_i^{\alpha,n}$ and $S_{i,j}^{\alpha,n}$ represent the subblocks at first and second level, respectively. The subscripts i and j are the indices for specifying the subblocks at first and second level, respectively, such that $i \in [1,4]$ and $j \in \begin{cases} [1,8], i = 1,2 \\ [1,6], i = 3,4 \end{cases}$

7: **for** each i^{th} subblock at the first-level of partitioning **do**

8: **for** each j^{th} subblock at the second-level of partitioning **do**

9: Calculate mean and standard deviations as per following equations [36]:

$$\mu_i^{\alpha,n} = \frac{\sum_{x,y} |S_i^{\alpha,n}(x,y)|}{m_i \times n_i}, \quad \mu_{ij}^{\alpha,n} = \frac{\sum_{x,y} |S_{ij}^{\alpha,n}(x,y)|}{m_{ij} \times n_{ij}}$$

$$\sigma_i^{\alpha,n} = \sqrt{\frac{\sum_{x,y} ||S_i^{\alpha,n}(x,y)| - \mu_i^{\alpha,n}|}{m_i \times n_i}}, \quad \sigma_{ij}^{\alpha,n} = \sqrt{\frac{\sum_{x,y} ||S_{ij}^{\alpha,n}(x,y)| - \mu_{ij}^{\alpha,n}|}{m_{ij} \times n_{ij}}}$$

▷ where (x,y) represents the pixel coordinates i.e. x^{th} row and y^{th} column. ▷ (m_i, n_i) are the dimensions of i^{th} first-level subblock and (m_{ij}, n_{ij}) are the dimensions of j^{th} second-level subblock in i^{th} first-level subblock.

10: **end for**

11: **end for**

12: Store the remainders after subtraction operation between standard deviations

$D^{\alpha,n} = [d_{11}^{\alpha,n} \mid d_{12}^{\alpha,n} \mid \cdots \mid d_{46}^{\alpha,n}]$

where, $d_{ij}^{\alpha,n} = \left|\sigma_i^{\alpha,n} - \sigma_{ij}^{\alpha,n}\right| \quad \forall (i,j)$ as explained in step 6

13: **end for**

14: **end for**

15: Concatenate all hybrid features to form the complete feature vector FV:

$FV = [D^{0,0} \mid D^{0,1} \mid \cdots \mid D^{4,3}]$

16: **return** FV

In the proposed approach, red channel of the input iris image is first extracted because red spectrum is closest to the NIR spectrum and hence represents the iris texture more clearly [32, 37]. This red channel image is then processed through Gabor wavelets of different frequencies, scales and orientations. This multi-scale and multi-resolution analysis of the iris image enables the proposed approach to extract wide-ranging features of iris. Thereafter, each wavelet-processed image is divided into subblocks using constant- and variable-size partitioning at first level and second level, respectively.

Means and standard deviations of all subblocks are then calculated. Standard deviation of the partitioned subblock is a clear measure of the intensity variations local to that subblock. In addition, when subtraction is performed between standard deviations of first- and corresponding second-level subblocks, the global variations

in the image intensities are nullified. This imparts illumination invariance to the proposed scheme. Additionally, subtraction of standard deviations of lower and higher-level subblocks is employed here for storing the relevant additional texture information which lower (or higher)-level subblocks possess with respect to the higher (or lower)-level subblocks. This additional relative texture information may be attributed to the presence of dense iris texture in some regions and absence of texture in the other regions, whereas absence of texture may be linked to the occlusion of iris texture through reflections, eyelids, and eyelashes. Therefore, mere standard deviations may lead to vague characterization of iris texture. This is the reason that the proposed feature extraction scheme employs subtraction of standard deviations to form the feature vector.

Moreover, since the subtraction of standard deviation is performed at varying scale and orientation of Gabor wavelets, the thin edges of iris texture dwelling in multiple directions contribute significantly to the overall feature vector. Therefore, the complete feature vector is constituted by concatenating the remainders of all subtraction operations, performed for the complete wavelet bank. This blend of textural and statistical characteristics provides discriminative property to the proposed hybrid features. Complete process of constructing the feature vectors is illustrated in Algorithm 1.

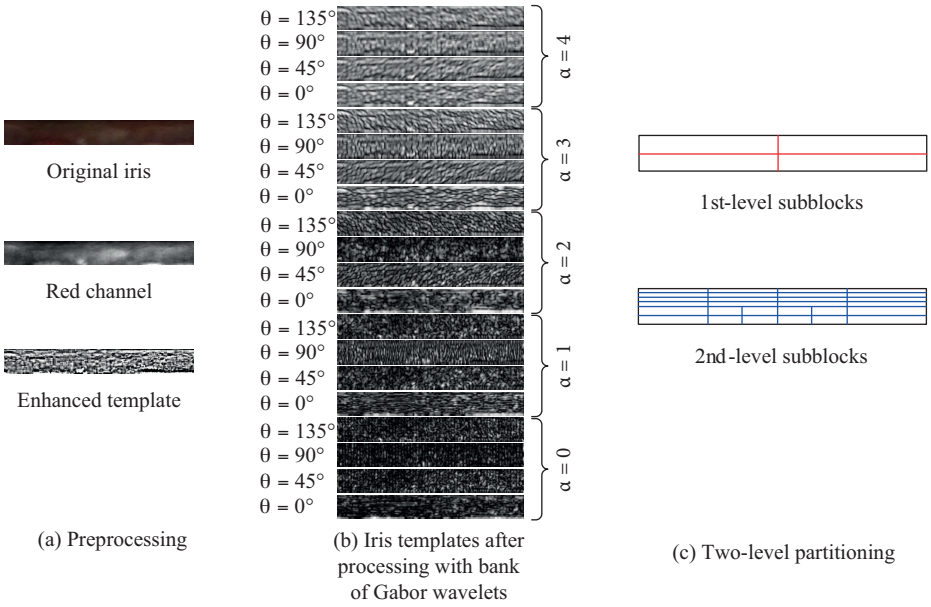

Figure 2. Schematic diagram of the proposed approach.

The schematic diagram of the proposed approach is shown in Figure 2. The original iris template is first enhanced to highlight its texture. This preprocessing is shown in Figure 2a while Figure 2b shows various instances of processing the input iris template through Gabor wavelets $\Gamma(\alpha, n)$. It can be visualized from Figure 2b how different scales of Gabor wavelets result in emergence of different texture patterns. This processing of iris template through the bank of Gabor wavelets provides multidimensionality and distinctiveness to the final feature vector. Finally, Figure 2c illustrates the division of Gabor-processed templates into two-level of subblocks: $S_i^{\alpha,n}$ and $S_{i,j}^{\alpha,n}$. It is also apparent from Figure 2c that the second-level subblocks have varying resolutions due to non-uniformity in their dimensions.

3.1. Feature vector size

As the proposed approach includes simple statistical formulae to constitute the feature vector, size of feature vector in this approach is also limited. Upon carefully observing the schematic diagram of the proposed approach (Figure 2), it can be inferred that that there are twenty different Gabor functions in total in the employed wavelet bank. Furthermore, each wavelet-processed image is divided into four and twenty-eight subblocks at the first- and second-level, respectively. Thereafter, standard deviation of each subblock is calculated and corresponding standard deviation values from first- and second-level subblocks are subtracted. Residues of these subtraction operations are stored in the form of a vector leading to twenty-eight values for one wavelet-processed image. In order to make these subtraction operations more apparent, the zoomed versions of one first-level subblock and eight second-level subblocks extracted from the selected first-level subblock are shown in Figure 3. The standard deviations of all these subblocks are also marked with appropriate subscripts. Now, in order to form the feature vector, the standard deviations of first- and second-level subblocks are subtracted as follows:

$$FV = [|\sigma_1 - \sigma_{11}|\,|\,|\sigma_1 - \sigma_{12}|\,|\cdots|\,|\sigma_1 - \sigma_{18}|\cdots] \tag{1}$$

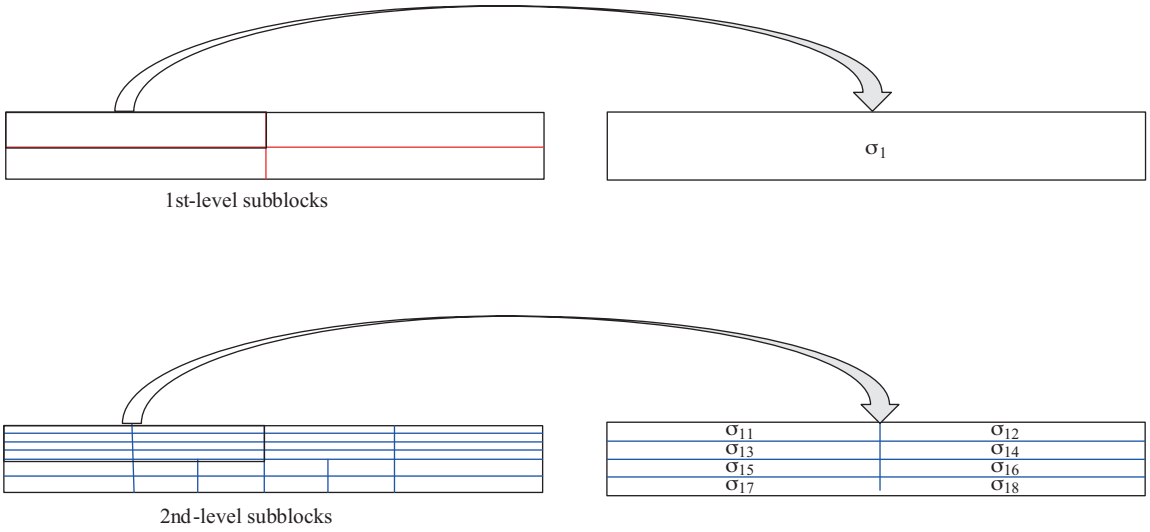

Figure 3. Standard deviations of different subblocks.

Therefore, it can be stated that features are formed by subtracting standard deviations of the second-level subblocks from the standard deviation of that first-level subblock, from which the second-level subblocks are extracted. Similarly, standard deviations of other second-level subblocks are subtracted from standard deviation of their respective first-level subblocks. Subsequently, completing all the wavelet-processed images leads to 560 (28×20) features, which is a very compact representation of the whole texture of iris when compared with other approaches (refer to Section 4.4 for discussion on comparison).

4. Performance evaluation

4.1. Experimental setup

The experiments in this research are carried out with a benchmark mobile iris database, called Mobile Iris CHallenge Evaluation (MICHE) (available at http://biplab.unisa.it/MICHE/index_miche.htm). This database was launched in order to evaluate iris segmentation and recognition techniques for smartphone-based systems

in MICHE I and MICHE II challenges, respectively. The database contains iris images captured from three different smartphone devices: iPhone5, Galaxy S4, and Galaxy Tab2 (written hereafter as IP5, GS4 and GT2, respectively). The whole database comprises 3190 iris images from 75 subjects, including at least 4 images per subject. Further, the images using IP5 and GS4 are acquired in four different frameworks using both rear and front cameras of the devices in indoor as well as outdoor illuminations. While for GT2 device, only front camera is used for acquisition.

The whole dataset is first segmented as per the method explained in Section 2. Thereafter, only those subjects that have at least four images with correctly localized iris boundaries are carefully selected for further processing. Moreover, only front camera images are considered here for the recognition purpose as it is quite impractical for a user to take his/her own eye image with rear camera of the device. Some sample images from the three devices are shown in Figure 4.

(a) IP5/outdoor (b) IP5/indoor (c) GS4/outdoor (d) GS4/indoor (e) GT2/outdoor (f) GT2/indoor

Figure 4. Sample images of the database acquired with the front cameras.

The performance of the proposed approach is assessed in terms of performance metrics like area under receiver operator characteristics curve (AUC), genuine acceptance rate (GAR), and equal error rate (EER). The GAR is observed at the specified EER for each experiment. Furthermore, experimentation is accomplished in two separate phases. The first phase helps in deciding the appropriate distance metric for the proposed approach while the second phase is responsible for corroborating the effective performance of the proposed approach through its comparison with other widespread approaches of iris recognition.

4.2. Phase I: Evaluation of distance metrics

This phase is aimed at selecting appropriate distance function for the addressed problem of mobile iris biometrics. The nearest neighbor classifier is employed in the proposed approach with three different distance functions namely city-block, Euclidean, and chi-square distance functions. Mathematical expressions of these distance functions are given in Eq. (2), where FV represents the feature vector extracted using the proposed approach, letters Q and G correspond to query and gallery images, respectively and L denotes the length of feature vector.

$$\begin{aligned} \text{City} - \text{block distance}: &\quad \sum_{i=1}^{L} |FV_{Q_i} - FV_{G_i}| \\ \text{Euclidean distance}: &\quad \sqrt{\sum_{i=1}^{L} (FV_{Q_i} - FV_{G_i})^2} \\ \text{Chi} - \text{square distance}: &\quad \frac{1}{2} \sum_{i=1}^{L} \frac{(FV_{Q_i} - FV_{G_i})^2}{FV_{Q_i} + FV_{G_i}} \end{aligned} \tag{2}$$

Choice of the distance function can significantly affect the overall accuracy of the recognition system.

This can also be verified by the values of performance metrics listed in Table 1 and graphs shown in Figures 5a and 5b (for indoor and outdoor environments, respectively). It can be ascertained from Table 1 and Figure 5 that the chi-square distance function outperforms the other two distance functions for indoor illuminated images. For IP5 database, the EER of chi-square distance metric turns out to be 0.0891 which is far below the EER achieved with city-block and Euclidean distances. Similarly, for GS4 and GT2 databases in indoor lighting conditions, EERs achieved with the proposed descriptor using chi-square distance metrics are 0.1496 and 0.1169, respectively. These values of EER are superior to those achieved with other two distance functions. Therefore, chi-square distance function is found suitable for the proposed descriptor in the indoor illumination framework.

Table 1. Comparison of different distance metrics.

Illumi.	Distance	IP5			GS4			GT2		
		AUC	GAR	EER	AUC	GAR	EER	AUC	GAR	EER
Indoor	City-block	0.9670	0.8958	0.1036	0.9032	0.8333	0.1678	0.9297	0.8708	0.1288
	Euclidean	0.9560	0.8917	0.1084	0.9015	0.8333	0.1687	0.9271	0.8625	0.1369
	Chi-square	0.9751	0.9083	0.0891	0.9143	0.8529	0.1496	0.9419	0.8833	0.1169
Outdoor	City-block	0.9146	0.8433	0.1589	0.9383	0.8625	0.1367	0.9209	0.8630	0.1370
	Euclidean	0.8931	0.8100	0.1886	0.9181	0.8375	0.1639	0.9100	0.8370	0.1617
	Chi-square	0.9223	0.8467	0.1526	0.9424	0.8583	0.1423	0.9342	0.8630	0.1375

Figure 5. Comparison of EER values of different distance metric for (a) indoor environment; (b) outdoor environment.

For outdoor illuminated images, city-block and chi-square distance metrics perform comparably for different smartphone devices. On the one hand, for IP5 device, chi-square distance function provides minimum EER (0.1526) among all three distance functions. On the other hand, for GS4 and GT2 devices, EERs obtained with city-block distance metric (0.1367 and 0.1370, respectively) remain the minimum. This varying performance of distance metrics may be attributed to the various challenges posed by the outdoor illumination framework. Due to this, the results of the proposed descriptor with outdoor illuminated images are specified with both the distance functions, city-block and chi-square.

4.3. Phase II: Comparison with other approaches

This phase of experimentation proves the efficacy of the proposed approach in smartphone-based iris matching framework. In this phase, images acquired from any one mobile device are matched against those acquired

Table 2. Comparative analysis of the proposed approach in indoor environment (using chi-square distance metric).

Illumi.	Approach	IP5			GS4			GT2		
		AUC	GAR	EER	AUC	GAR	EER	AUC	GAR	EER
Indoor	BLPOC	0.7981	0.7375	0.2667	0.6800	0.6119	0.3887	0.7666	0.7000	0.2990
	DCT	0.8481	0.7792	0.2213	0.7942	0.7108	0.2886	0.7745	0.6958	0.3018
	IrisCode	**0.9874**	**0.9458**	**0.0527**	0.9322	0.8480	0.1505	0.9167	0.8417	0.1593
	Haralick	0.8647	0.7625	0.2312	0.8704	0.8088	0.1769	0.8451	0.7708	0.2185
	XorSum	0.9729	0.9292	0.0720	0.9004	0.8382	0.1574	0.9453	**0.8917**	**0.1104**
	Statistical	0.9756	0.9292	0.0714	**0.9382**	**0.8676**	**0.1313**	**0.9520**	0.8833	0.1171
	Log-Gabor	0.9808	0.9333	0.0662	0.9286	0.8627	0.1370	0.9313	0.8625	0.1368
	RINBP	0.9372	0.8792	0.1203	0.9276	0.8578	0.1421	0.9463	0.8792	0.1193
	Proposed	**0.9751**	**0.9083**	**0.0891**	**0.9143**	**0.8529**	**0.1496**	**0.9419**	**0.8833**	**0.1169**

from the same device. Tables 2 and 3 show the values of performance metrics, AUC, GAR and EER, for the proposed as well as other standard approaches in indoor and outdoor environments, respectively. The best values of performance metrics, along with the metrics of the proposed approach, are highlighted by bold characters in Tables 2 and 3. Here the proposed approach is compared with various benchmark approaches like BLPOC [12], DCT [11], IrisCode [1], Haralick [20], XorSum [18], statistical [19], log-Gabor [22], and rotation invariant neighborhood-based binary pattern (RINBP) [23]. The feature extraction approaches in [20] and [23] (i.e. Haralick and RINBP) are implemented along with chi-square and Euclidean distance metrics, respectively. Figures 6 and 7 depict this comparison using bar-charts, for indoor and outdoor illumination environments, respectively.

While analyzing the functioning of the proposed approach in indoor environments (Table 2), it is found that the proposed approach is performing poor or comparable to the other existing approaches. For IP5 device, EER achieved in the proposed approach (0.0891) is worse than IrisCode (0.0527), XorSum (0.0720), statistical (0.0714), and log-Gabor (0.0662) approaches. This may be attributed to the high resolution of database images. However, it may sound interesting to the reader that the proposed approach is yielding such comparable performance with a small feature vector size (kindly refer to Section 4.4 for more detailed discussion on feature vector size). On the other hand, the proposed approach outperforms IrisCode and XorSum approaches for GS4 database, in terms of EER. However, it still performs comparable to statistical, log-Gabor, and RINBP approaches while, for GT2 database, performance of the proposed approach (in terms of EER) is at par with respect to all other listed approaches except XorSum. To be precise, EER of the proposed approach is 0.1169, which is the second best after that of XorSum (0.1104). However, the proposed approach has supremacy over XorSum in terms of feature extraction speed i.e. speed of the proposed approach is almost double of that yielded by XorSum (refer to Section 4.5 for details). Pictorial comparisons of the performance metrics for matchings in indoor environment for IP5, GS4, and GT2 devices are also shown in Figures 6a–6c), respectively.

Furthermore, it is important to note here that despite poor or comparable performance of the proposed approach in indoor illumination, it solves the major challenge of feature vector size. Since smartphones have limited storage capacity and computation power, feature descriptors yielding huge-sized feature vectors are not suitable for them. Therefore, approaches like IrisCode and Log-Gabor, which otherwise produce good performance, are not suitable to be implemented on smartphones because of their huge feature vector size. On

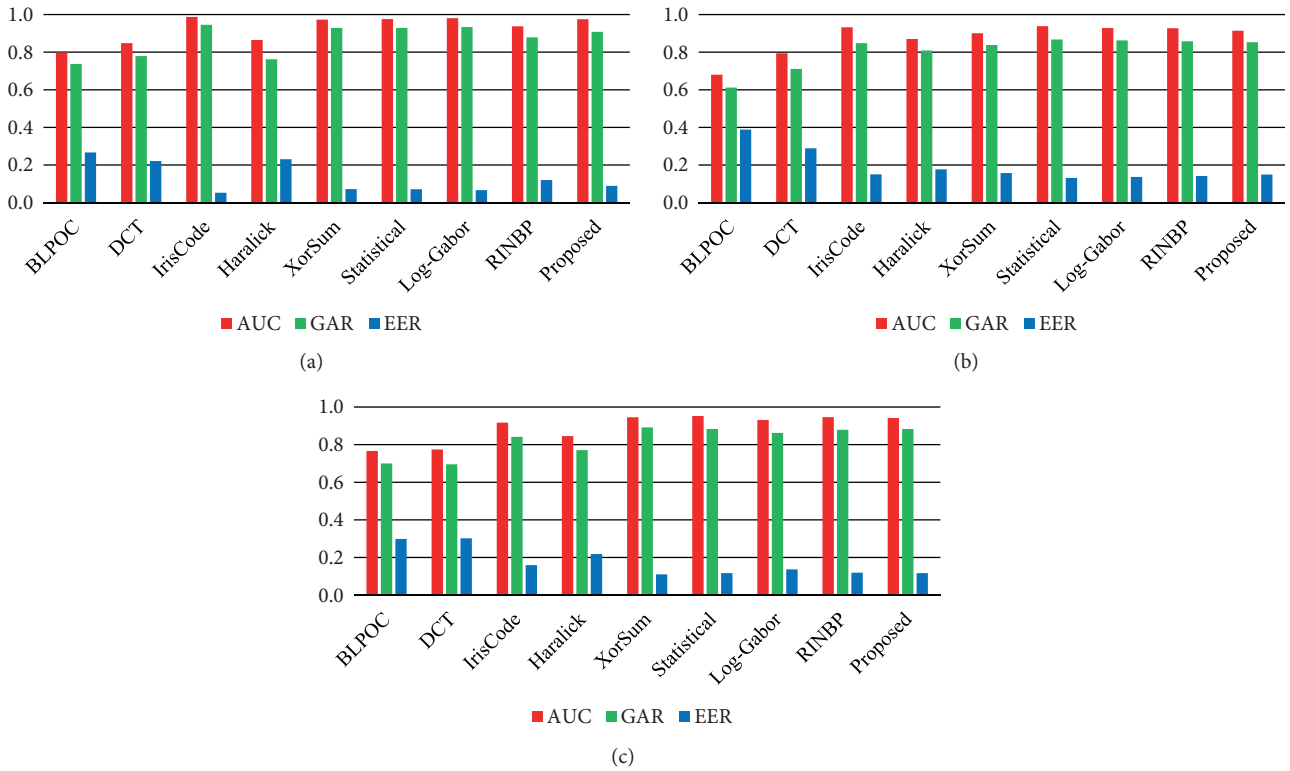

Figure 6. AUC, GAR, and EER comparisons of the proposed approach in indoor environments for (a) IP5, (b) GS4, and (c) GT2 device.

the contrary, the proposed approach involves limited feature vector size and simple computations, which makes it suitable for the said application of smartphone-based iris recognition.

Table 3. Comparative analysis of the proposed approach in outdoor environment.

Illumi.	Approach	IP5			GS4			GT2		
		AUC	GAR	EER	AUC	GAR	EER	AUC	GAR	EER
Outdoor	BLPOC	0.8301	0.7567	0.2397	0.5815	0.5395	0.4613	0.6475	0.6000	0.3982
	DCT	0.7753	0.7000	0.2958	0.5196	0.4792	0.5135	0.5302	0.5167	0.4807
	IrisCode	0.8952	0.8067	0.1926	0.6456	0.5833	0.4112	0.6200	0.5762	0.4245
	Haralick	0.8391	0.7567	0.2385	0.8594	0.7750	0.2210	0.8807	0.8074	0.1957
	XorSum	0.8830	0.8100	0.1907	0.6164	0.5750	0.4298	0.6576	0.6097	0.3880
	Statistical	**0.9249**	**0.8467**	**0.1525**	0.9090	0.8375	0.1609	0.9281	0.8519	0.1468
	Log-Gabor	0.8890	0.8067	0.1926	0.8392	0.7458	0.2529	0.8992	0.8222	0.1753
	RINBP	0.8951	0.8200	0.1810	0.9312	0.8542	0.1445	0.9155	0.8407	0.1595
	Proposed (with City-block)	**0.9146**	**0.8433**	**0.1589**	**0.9383**	**0.8625**	**0.1367**	**0.9209**	**0.8630**	**0.1370**
	Proposed (with chi-square)	**0.9223**	**0.8467**	**0.1526**	**0.9424**	**0.8583**	**0.1423**	**0.9342**	**0.8630**	**0.1375**

When it comes to the performance evaluation of various feature extraction approaches in outdoor environments, the proposed approach clearly outperforms all the listed state-of-the-art approaches, as is evident from Table 3. This table indicates the performance of the proposed approach with two distance metrics, namely city-block and chi-square, as both these metrics are yielding comparable results. Although the outdoor images have huge texture variations, the proposed approach is able to represent them distinctively, unlike other ap-

proaches. On observing the performance of the proposed approach for IP5 device in outdoor environment, it can be clearly noticed that all three performance metrics are significantly superior (comparable to Statistical approach though) as compared to those of other benchmark approaches. Same argument applies to other two devices, GS4 and GT2, for outdoor illumination experiments. In addition, preponderance of the proposed approach in outdoor illumination framework is illustrated by Figure 7. It can be clearly observed from Figures 7a–7c) that the proposed approach performs efficiently for all three devices.

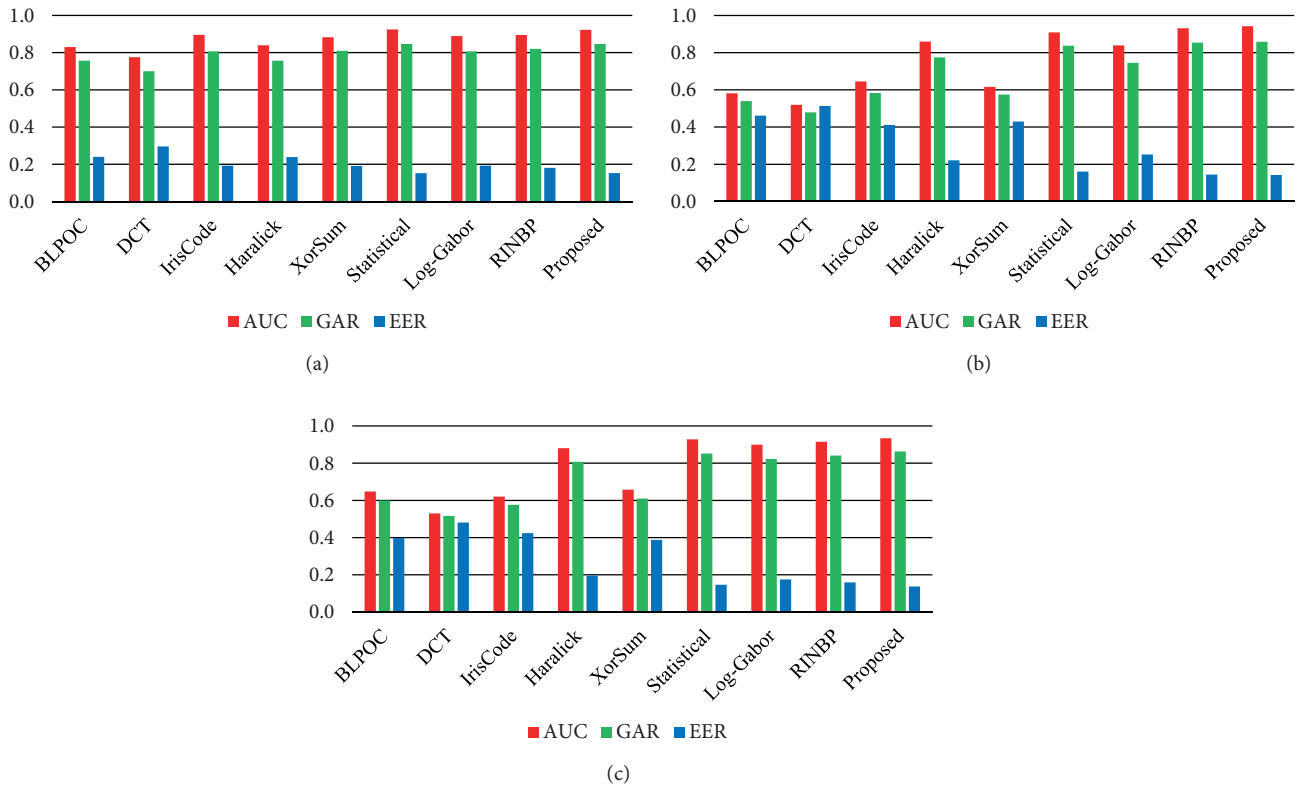

Figure 7. AUC, GAR and EER comparisons of the proposed approach in outdoor environments for (a) IP5; (b) GS4; and (c) GT2 device.

4.4. Comparison of feature vector size

In view of this comparison, Table 4 furnishes the details of size that each feature vector occupies in the MATLAB workspace (since BLPOC is a phase-based matcher, no feature vector size is indicated for it). These sizes are obtained by using *whos* function of MATLAB. It can be observed from Table 4 that feature vector size of the proposed approach, is far less than most of the listed approaches, except Haralick and RINBP. Out of these two approaches, Haralick approach produces equal feature vector size as that of the proposed approach while RINBP is yielding slightly lesser feature vector size as compared to that of the proposed approach. Therefore, the superiority of the proposed approach in terms of feature vector size can be established from Table 4.

4.5. Comparison of feature extraction speed

This subsection deals with the comparison of time elapsed in feature extraction process of the proposed descriptor and other state-of-the-art descriptors. All the descriptors were implemented on a Windows-based system having

Table 4. Comparison of feature vector size.

Approach	BLPOC	DCT	IrisCode	Haralick	XorSum	Statistical	Log-Gabor	RINBP	Proposed
Feature vector size (KB/image)	–	32	512	4.375	48	26.9063	128	4	4.375

i7@3.40 GHz processor and 8 GB RAM. The platform used for coding is MATLAB R2016a. Table 5 lists the feature extraction speed in *sec/image* for all the employed descriptors. Since BLPOC is a phase-based matcher, no feature extraction time is indicated for it. Furthermore, speed of the proposed feature descriptor is the second fastest after that of log-Gabor–based descriptor, which takes 126 ms for one image with respect to the 143 ms per image taken by the proposed descriptor while all other descriptors have higher feature-extraction time or lower feature-extraction speed when compared with those of the proposed descriptor. Therefore, the proposed descriptor can prove to be a suitable candidate for real-time iris recognition systems.

Table 5. Comparison of feature extraction speed.

Approach	BLPOC	DCT	IrisCode	Haralick	XorSum	Statistical	Log-Gabor	RINBP	Proposed
Time elapsed *(sec/image)*	—	0.211	0.259	2.246	0.270	0.189	0.126	0.299	0.143

5. Conclusions

This paper presents a hybrid feature extraction approach to be used in mobile iris biometrics. The proposed approach uses 2D Gabor wavelets and standard deviation formulae to achieve the feature extraction. Multiscale and multiresolution analysis of iris templates through Gabor wavelets ensure the highlighting of wide-ranging texture present in the iris. Then, breakdown of iris templates into subblocks at two separate levels aids in capturing the local textural features. The intensive experimentation performed on the challenging MICHE mobile iris database proves the usefulness of the proposed approach. It can be observed that the proposed approach outperforms the state-of-the-art approaches in terms of all reported performance metrics, especially in the outdoor illumination environment, which is the more challenging among both types of illumination.

Acknowledgment

The authors wish to thank Biometric and Image Processing Lab (BIPLab) at University of Salerno, Fisciano, Italy, for making their mobile iris database available for research.

References

[1] Daugman JG. High confidence visual recognition of persons by a test of statistical independence. IEEE T Pattern Anal 1993; 15: 1148-1161.

[2] Daugman J. Iris recognition at airports and border crossings. In: Li SZ, Jain AK, editors. Encyclopedia of Biometrics. Boston, MA, USA: Springer; 2015. pp. 998-1004.

[3] Abdullah MAM, Al-Nima RR, Dlay SS, Woo WL, Chambers JA. Cross-spectral iris matching for surveillance applications. In: Karampelas P, Bourlai, T, editors. Surveillance in Action, Advanced Sciences and Technologies for Security Applications. Cham, Cham, Switzerland: Springer; 2018. pp. 105-125.

[4] Jain AK, Ross A, Prabhakar S. An introduction to biometric recognition. IEEE T Circ Syst Vid 2004; 14: 4-20.

[5] Bowyer KW, Hollingsworth K, Flynn PJ. Image understanding for iris biometrics: a survey. Comput Vis Image Und 2008; 110: 281-307.

[6] Basit A, Javed MY. Localization of iris in gray scale images using intensity gradient. Opt Laser Eng 2007; 45: 1107-1114.

[7] Wildes RP, Asmuth JC, Green GL, Hsu SC, Kolczynski RJ, Matey JR, McBride SE. A system for automated iris recognition. In: Proceedings of the Second IEEE Workshop on Applications of Computer Vision; 5-7 Dec 1994; Sarasota, FL, USA. New York, NY, USA: IEEE. pp. 121-128.

[8] Flom L, Safir A. Iris recognition system, US Pat 4,641,349. 1987.

[9] Masek L, Kovesi P. MATLAB source code for a biometric identification system based on iris patterns. The School of Computer Science and Software Engineering, The University of Western Australia, Perth, Australia, 2003.

[10] Ganeshan B, Theckedath D, Young R, Chatwin C. Biometric iris recognition system using a fast and robust iris localization and alignment procedure. Opt Laser Eng 2006; 44: 1-24.

[11] Monro DM, Rakshit S, Zhang D. DCT-based iris recognition. IEEE T Pattern Anal 2007; 29: 586-595.

[12] Miyazawa K, Ito K, Aoki T, Kobayashi K, Nakajima H. An effective approach for iris recognition using phase-based image matching. IEEE T Pattern Anal 2008; 30: 1741-1756.

[13] Rai H, Yadav A. Iris recognition using combined support vector machine and Hamming distance approach. Expert Syst Appl 2014; 41: 588-593.

[14] Tan C-W, Kumar A. Efficient and accurate at-a-distance iris recognition using geometric key-based iris encoding. IEEE T Inf Forensics 2014; 9: 1518-1526.

[15] Tan C-W, Kumar A. Accurate iris recognition at a distance using stabilized iris encoding and Zernike moments phase features. IEEE T Image Process 2014; 23: 3962-3974.

[16] Bhateja AK, Sharma S, Chaudhury S, Agrawal N. Iris recognition based on sparse representation and k-nearest subspace with genetic algorithm. Pattern Recogn Lett. 2015; 73: 13-18.

[17] Umer S, Dhara BC, Chanda B. Iris recognition using multiscale morphologic features. Pattern Recogn Lett 2015; 65: 67-74.

[18] Vyas R, Kanumuri T, Sheoran G. Iris recognition using 2-D Gabor filter and XOR-SUM code. In: 2016 1st India International Conference on Information Processing; 12-14 Aug 2016; Delhi, India: IEEE. pp. 1-5.

[19] Bansal M, Hanmandlu M, Kumar P. Iris based authentication using local principal independent components. Optik 2016; 127: 4808-4814.

[20] Subban R, Susitha N, Mankame DP. Efficient iris recognition using Haralick features based extraction and fuzzy particle swarm optimization. Cluster Comput. 2017; 21: 1-12.

[21] Bansal A, Agarwal R, Sharma RK. Statistical feature extraction based iris recognition system. Sādhanā 2016; 41: 507-518.

[22] Poornima S, Subramanian S. Unconstrained iris authentication through fusion of RGB channel information. Int J Pattern Recogn 2014; 28: 1456010-1-18.

[23] Hamouchene I, Aouat S. Efficient approach for iris recognition. Signal Image Video P 2016; 10: 1361-1367.

[24] Vyas R, Kanumuri T, Sheoran G, Dubey P. Co-occurrence features and neural network classification approach for iris recognition. In: 2017 Fourth International Conference on Image Information Processing; 21-23 Dec 2017; Solan, India: IEEE. pp. 1-6.

[25] De Marsico M, Nappi M, Riccio D, Wechsler H. Mobile Iris Challenge Evaluation (MICHE)-I, biometric iris dataset and protocols. Pattern Recogn Lett 2015; 57: 17-23.

[26] De Marsico M, Nappi M, Proença H. Results from MICHE II – mobile iris challenge evaluation II. Pattern Recogn Lett 2017; 91: 3-10.

[27] Abate AF, Barra S, Gallo L, Narducci F. Kurtosis and skewness at pixel level as input for SOM networks to iris recognition on mobile devices. Pattern Recogn Lett 2017; 91: 37-43.

[28] Barra S, Casanova A, Narducci F, Ricciardi S. Ubiquitous iris recognition by means of mobile devices. Pattern Recogn Lett 2015; 57: 66-73.

[29] Galdi C, Nappi M, Dugelay JL. Multimodal authentication on smartphones: Combining iris and sensor recognition for a double check of user identity. Pattern Recogn Lett 2016; 82: 144-153.

[30] Viola P, Jones M. Rapid object detection using a boosted cascade of simple features. In: Proceedings of the 2001 IEEE Computer Society Conference on Computer Vision and Pattern Recognition; 8-14 Dec 2001; Kauai, HI, USA: IEEE. pp. 511-518.

[31] Viola P, Jones M. Robust real-time face detection. Int J Comput Vision 2004; 57: 137-154.

[32] Zhao Z, Kumar A. An accurate iris segmentation framework under relaxed imaging constraints using total variation model. In: IEEE International Conference on Computer Vision; 7-13 Dec. 2015; Santiago, Chile. New York, NY, USA: IEEE. pp. 3828-3836.

[33] Brainard DH, Wandell BA. Analysis of the retinex theory of color vision. J Opt Soc Am A. 1986; 3: 1651-1661.

[34] Wildes RP. Iris recognition: an emerging biometric technology. P IEEE 1997; 85: 1348-1363.

[35] Daugman J. The importance of being random: statistical principles of iris recognition. Pattern Recogn 2003; 36: 279-291.

[36] Arivazhagan S, Ganesan L, Priyal SP. Texture classification using Gabor wavelets based rotation invariant features. Pattern Recogn Lett 2006; 27: 1976-1982.

[37] Tan C-W, Kumar A. Unified framework for automated iris acquired face images. IEEE T Image Process 2012; 21: 4068-4079.